Development and implementation of shear wall finite element in OpenSees

Engineering Structures 304 (2024) 117639

Contents lists available at ScienceDirect

Engineering Structures

journal homepage: www.elsevier.com/locate/engstruct

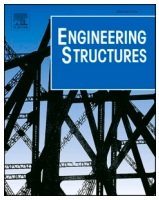

Development and implementation of shear wall finite element in OpenSees

Minsheng Guan [a], Xiru Hang [a], Mengsen Wang [a], Hanyuan Zhao [a], Qing Quan Liang [b,*,1], Ying Wang [c]

[a] Key Laboratory of Coastal Urban Resilient Infrastructures at Shenzhen University, Ministry of Education, Shenzhen 518060, China
[b] College of Sport, Health, and Engineering, Victoria University, PO Box 14428, Melbourne, VIC 8001, Australia
[c] College of Civil Engineering, Fuzhou University, Fuzhou 350116, China

ARTICLE INFO

Keywords:
Double Vertical Beam-column with Shell Element
Finite element analysis
Numerical simulation
Shear walls

ABSTRACT

Shear walls are widely used as lateral load-resisting systems in high-rise building structures. The design and nonlinear analysis of shear walls under seismic loads for recoverability are complicated and challenging, which demands nonlinear computer modeling procedures. This paper presents a novel finite element named Double Vertical Beam-column with Shell Element (DVBSE) for the nonlinear analysis of complex reinforced concrete shear walls with columns. The DVBSE is implemented in the open-source finite element program OpenSees. The theoretical formulations of DVBSE are described in detail. The accuracy of the developed DVBSE is established by comparing the finite element analysis results with existing experimental data on recoverable steel-GFRP composite bar reinforced concrete shear walls. The comparative study demonstrates that the proposed DVBSE is superior to the commonly used finite element model in simulating the responses of recoverable complex shear walls under seismic loads. These research findings contribute to further advancements in the development of new shear wall elements and lay a solid foundation for the nonlinear numerical simulation of innovative shear walls.

1. Introduction

Earthquakes can result in urban dysfunction through structural damage to buildings, resulting in considerable detriment to public infrastructure and the loss of human life. Prompt restoration of building functionality after earthquake is crucial to mitigate losses and expedite urban recovery [1]. Shear walls are commonly employed in building structures to resist earthquakes. Recoverable structures, which can regain their functionality after an earthquake without repair or with only minor repairs, have been studied by Fragiadakis et al. [2], Yang et al. [3], Deng et al. [4], Rong [5], and Eatherton et al. [6]. Most existing recoverable structures utilize self-centering mechanisms that allow for rocking [6–10]. Establishing an accurate finite element (FE) model of recoverable new shear walls is challenging. Presently, existing finite elements cannot accurately model the measured responses of novel shear walls made of new materials or structural elements due to complex stress states in such shear walls [11–13]. Therefore, it is necessary to develop a new element that is capable of accurately simulating the responses of these shear walls as discussed by Chang et al. [14].

The finite element method is widely used in the numerical analysis of engineering structures [15]. Finite element models for shear walls primarily consist of micro-models and macro-models [14]. Micro-element models involve dividing the structure into numerous small entities for individual force analysis, later integrating these results to derive the overall structure's force analysis as reported by Guan et al. [16]. Examples include the solid element model and the fiber-based beam model (each fiber can individually specify equilibrium conditions, suitable for small displacement analysis), which typically necessitate grid division for calculation. Micro-element models are generally employed for the analysis of structural members under complex loads [17]. However, micro-models have drawbacks, including complex modeling, lengthy calculation times, low efficiency, and convergence issues. Consequently, micro-models are typically used for supplementary analysis of single components under complex load. In micro-element models, achieving accurate results requires balancing precision and computational efficiency. Conversely, fiber-based beam models lack consideration of shear and bonding sliding between fibers, potentially leading to shear-bending decoupling. Macro-element models, such as equivalent beam models, demonstrate high efficiency in calculating the stress state of simple shear

* Corresponding author.
E-mail address: Qing.Liang@vu.edu.au (Q.Q. Liang).
[1] https://orcid.org/0000-0003-0333-2265

https://doi.org/10.1016/j.engstruct.2024.117639
Received 9 November 2023; Received in revised form 13 January 2024; Accepted 7 February 2024
Available online 20 February 2024

walls but face challenges in accurately representing the stress state of novel complex shear walls. The reliability of multi-vertical rod models depends on available experimental data; without it, obtaining precise results is challenging. Shear plate models, while improving the precision of coupling between bending and shearing under high shear stress, exhibit significant limitations in terms of loading conditions as reported by Yam et al. [18] and Kolozvari et al. [19]. Shell models provide satisfactory simulation accuracy and relatively high computational efficiency, yet they lack the capability to simulate the edge region of complex shear walls. Truss elements are simple to model and easy to calculate but pose significant constraints when employed for non-elastic analyses [20,21].

In summary, the various element models discussed above exhibit relatively good applicability to traditional, simple structures. However, these models have limitations in delivering precise and efficient simulations, especially when dealing with the complexity of self-centering shear walls. There is a critical need to improve finite element analysis methods to address the complex stress states in these novel shear walls [14].

This paper introduces an innovative finite element, DVBSE (Double Vertical Beam-column with Shell Element), designed to simulate a new type of recoverable shear walls, as illustrated in Fig. 1. The DVBSE's edge region is constructed using fiber-based beam-column models based on the stiffness method on both sides, addressing the complex edge region of the shear wall, which cannot be simulated by shell elements. The middle part employs a shell element with excellent coupling performance between bending and shearing, achieving stress transfer by node sharing. DVBSE has several key features that underscore its innovation: (1) suitability for finite element analysis of novel and complex shear walls, with a specific focus on capturing the intricate stress characteristics of the edge constraint region; (2) implementing deformation coordination; (3) effective management of complex boundaries, simplification of modeling methods, and a demonstration of robust convergence and computational precision.

The development of DVBSE is primarily driven by the constraints inherent in conventional simulation methods. DVBSE stands as a pioneering solution for the simulation of self-centering shear walls. Its comprehensive design, integrating fiber-based beam-column model and a coupling-efficient shell element, enables a nuanced exploration of complex stress characteristics.

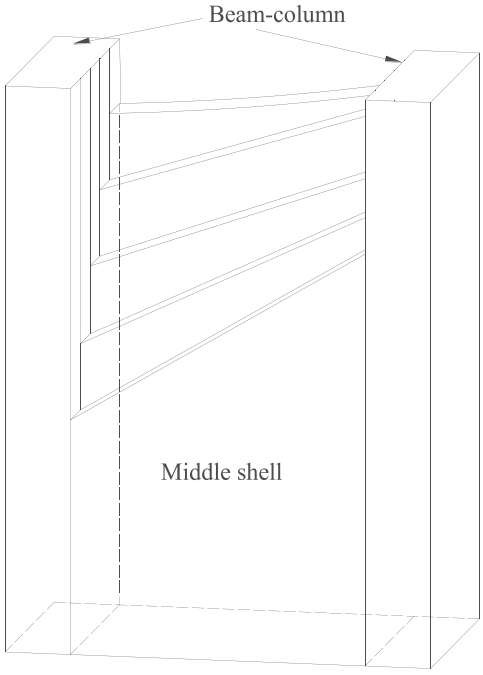

Fig. 1. Double Vertical Beam-column with Shell Element.

The DVBSE has been developed and implemented on the OpenSees platform. The paper is organized as follows. The theoretical formulation of DVBSE is described in Section 2. This is followed by the implementation of the shear wall element in OpenSees in Section 3. Section 4 presents the verification by experimental results on new shear walls. Concluding remarks are given in Section 5. While a comprehensive comparative study on the efficiency of DVBSE and other elements has been undertaken, this paper does not include a detailed comparison due to page limitation.

2. Theoretical formulation of DVBSE

2.1. General

The DVBSE is developed to simulate the shear wall, where a high-performance quadrilateral flat shell element NLDKGQ which is based on DKGQ is utilized to model the web and a fiber-based beam-column model is used to simulate the constrained edge components. DKGQ demonstrates superior computational accuracy and avoids locking issues, compared to MITC4 shell element in OpenSees. Additionally, DKGQ's computational results closely align with the accuracy of S4 element in ABAQUS. [22] The DVBSE is suitable for the analysis of complex novel shear walls: (1) using complex materials in the constrained edge region; (2) complex base structure of the wall; (3) intricate web of the shear wall.

In DVBSE, the high-performance quadrilateral plate shell (NLDKGQ) model is formulated based on the stiffness method, which significantly improves the advantage of the DVBSE. On the other hand, the shear wall edge constraint region is modeled using a fiber equivalent beam element which can accurately model the complex state of edge forces as discussed by Kolozvari et al. [23]. Considering these features, the basic theory of the DVBSE must address three fundamental issues: boundary constraint handling, external load handling, and stiffness matrix assembly.

2.2. Boundary constraint handling

In the DVBSE model, four edge constraints are considered, which include the junction between the fiber beam and the shell, as well as the top and bottom of the wall. With regards to the bottom of the wall, a handling method that employs full constraint is directly utilized in order to represent the actual stress state of the shear wall. In contrast, a load constraint handling method is employed for the top of the wall.

The junction between the fiber beam and the shell is a relatively complex area, as both must bear loads and deform. OpenSees provides the equalDOF and rigidLink methods to handle the problem of node movement along with the main node. However, due to the uniform constraints in the double perpendicular beam shell element, these methods are not used. The node that first generates displacement is automatically considered as the main node, while the others are considered as the slave nodes. Once the load is further transmitted to the slave nodes, the displacement at the slave node can be divided into two parts: the displacement caused by the main node and the displacement caused by the load directly. The difference between these two can be used to determine the convergence of the calculation. By utilizing this theory, both the main and slave nodes possess flexibility, changing as the program changes and providing a preliminary judgment of the displacement order of the nodes. The convergence of the calculation is determined by comparing the displacement caused by the main node. This additional judgment condition imposed during the iteration process theoretically has a minimal effect on the entire computational process.

2.3. External load handling

The FE model is proposed for the nonlinear analysis of complex shear walls subjected to vertical loads on the top of the shear walls. In the finite element analysis process, it is necessary to ensure that the loads are uniformly distributed to each node. Referring to the multi-vertical rod model, a rigid beam can be applied at the top to ensure the uniform distribution of loads. However, in the double perpendicular beam shell element model, constraints have already been imposed at the interface, minimizing the impact of a rigid beam on the overall model. Consequently, in the double perpendicular beam shell model, the top rigid beam is not included by default. If the user is concerned about the convergence of the overall model, they can add a rigid beam.

2.4. DVBSE stiffness matrix assembly

The stiffness matrices $\boldsymbol{K}_{DKQ}$ of the quadrilateral thin plate bending element DKQ and $\boldsymbol{K}_{GQ12}$ of the quadrilateral planar membrane element GQ12, as given in Eq. (1) and Eq. (2), can be decomposed into matrix form according to Eq. (3) and Eq. (4).

$$\boldsymbol{K}_{DKQ(16*16)} = \begin{bmatrix} k_{1,1} & \cdots & k_{1,16} \\ \vdots & \ddots & \vdots \\ k_{16,1} & \cdots & k_{16,16} \end{bmatrix} \# \tag{1}$$

$$\boldsymbol{K}_{GQ12(12*12)} = \begin{bmatrix} k_{1,1} & \cdots & k_{1,12} \\ \vdots & \ddots & \vdots \\ k_{12,1} & \cdots & k_{12,12} \end{bmatrix} \# \tag{2}$$

$$\boldsymbol{K}_e^{DKT} = 2A \int_0^1 \int_0^{1-\eta} \boldsymbol{B}_{DKT}^T \boldsymbol{D}_b \boldsymbol{B}_{DKT} \mathrm{d}\xi \mathrm{d}\eta \# \tag{3}$$

$$\boldsymbol{K}_e^{\mathrm{GQ12}} = t \iint_{A^e} \boldsymbol{B}^{\mathrm{T}} \boldsymbol{D} \boldsymbol{B} \mathrm{d}A = t \int_{-1}^1 \int_{-1}^1 \boldsymbol{B}^{\mathrm{T}} \boldsymbol{D} \boldsymbol{B} |j| \mathrm{d}\xi \mathrm{d}\eta \# \tag{4}$$

In Eq. (3) and Eq. (4), the detailed formulas of various parameters can be found in the work by Noh et al. [24].

In Eq. (1), each value of k is calculated according to equation Eq. (3), with a total of 16 rows and 16 columns. For each node, the first and second terms are the contributions of translational degrees of freedom in the plane, and the third and fourth terms are the contributions of rotational degrees of freedom in the plane.

In Eq. (2), each value of k is calculated according to equation Eq. (4), with a total of 12 rows and 12 columns. For each node, the first and second terms are the translational degrees of freedom resulting from the combination of the initial displacement field and the additional displacement field, including one term for in-plane translational degrees of freedom and one term for out-of-plane translational degrees of freedom. The third term is the contribution of in-plane rotational degrees of freedom from the additional displacement field.

Let $\mathbf{T}_{\mathrm{DKQ}(24*16)}$ be the transformation matrix from DKQ to the global coordinate system. The transformed stiffness matrix $\mathbf{K}_{\mathrm{DKQ}}^{\mathrm{e}}$ is obtained by filling in the unspecified elements in $\mathbf{K}_{\mathrm{DKQ}}$ with 0's and then performing the transformation:

$$\boldsymbol{K}_{DKQ}^e = \boldsymbol{T}_{DKQ}^T * \boldsymbol{K}_{DKQ} * \boldsymbol{T}_{DKQ} \# \tag{5}$$

Let $\mathbf{T}_{\mathrm{GQ12}(24*15)}$ be the transformation matrix from GQ12 part to the global coordinate system. The transformed stiffness matrix $\boldsymbol{K}_{GQ12}^e$ is obtained by filling in the unspecified elements in $\boldsymbol{K}_{GQ12}$ with 0's and then performing the transformation:

$$\boldsymbol{K}_{GQ12}^e = \boldsymbol{T}_{GQ12}^T * \boldsymbol{K}_{GQ12} * \boldsymbol{T}_{GQ12} \# \tag{6}$$

The high-performance quadrilateral plate shell element DKGQ is obtained by combining the quadrilateral thin plate bending element DKQ and the quadrilateral plane membrane element GQ12. The overall stiffness matrix $\boldsymbol{K}_{DKGQ}$ is

$$\boldsymbol{K}_{DKGQ(24*24)} = \boldsymbol{K}_{DKQ}^e + \boldsymbol{K}_{GQ12}^e = \begin{bmatrix} k_{1,1} & \cdots & k_{1,24} \\ \vdots & \ddots & \vdots \\ k_{24,1} & \cdots & k_{24,24} \end{bmatrix} \# \tag{7}$$

The stiffness matrix $\boldsymbol{K}_{DKGQ}$ has 24 rows and 24 columns, with each node's stiffness matrix including the first three terms representing translational degrees of freedom and the last three terms representing rotational degrees of freedom.

The nonlinear beam-column element stiffness matrix $\boldsymbol{K}_{DBC}$ based on the stiffness method is decomposed in the form of matrix as

$$K_{DBC(12*12)} = \begin{bmatrix} k_{1,1} & \cdots & k_{1,24} \\ \vdots & \ddots & \vdots \\ k_{24,1} & \cdots & k_{24,24} \end{bmatrix} \# \tag{8}$$

Let $\boldsymbol{T}_{DBC(24*12)}$ be the transformation matrix from the $\boldsymbol{K}_{DBC}$ part to the global frame, with the unrepresented quantities in $\boldsymbol{K}_{DBC}$ filled in with zeros. The transformed stiffness matrix is $\boldsymbol{K}_{DKQ}^e$:

$$\boldsymbol{K}_{DBC}^e = \boldsymbol{T}_{DBC}^T * \boldsymbol{K}_{DBC} * \boldsymbol{T}_{DBC} \# \tag{9}$$

A high-performance quadrilateral plate shell element DKGQ and a nonlinear beam-column element based on stiffness method are integrated. There are m longitudinal and n horizontal DKGQs, and m stiffness method beam-column elements on both sides. The main node of DKGQ is used as the node and the overall stiffness matrix of DVBSE ($\boldsymbol{K}_{TVBSE}$) is obtained through the common node method as shown in Eq. (10), where $k_{x,y}^{DKGQ_{i,j}}$ represents the value at position (x,y) in the stiffness matrix of the DKGQ element at position (i,j) and $\boldsymbol{K}_{(i,j)}^{DBC}$ represents the stiffness matrix at position (i,j).

$$\boldsymbol{K}_{TVBSE} = \begin{bmatrix} \boldsymbol{K}_{11} & \cdots & \boldsymbol{K}_{1j} & \cdots & \boldsymbol{K}_{1n} \\ \vdots & & \vdots & & \vdots \\ \boldsymbol{K}_{i1} & \cdots & \boldsymbol{K}_{ij} & \cdots & \boldsymbol{K}_{in} \\ \vdots & & \vdots & & \vdots \\ \boldsymbol{K}_{m1} & \cdots & \boldsymbol{K}_{mj} & \cdots & \boldsymbol{K}_{mn} \end{bmatrix} \# \tag{10}$$

where

$$\begin{aligned} \boldsymbol{K}_{11} &= \&\left(\boldsymbol{K}_{(1,1)}^{DBC}\right)^T * \boldsymbol{K}_{(1,1)}^{DKGQ} * \boldsymbol{K}_{(1,1)}^{DBC} \\ &+\&\left(\boldsymbol{K}_{(1,2)}^{DKGQ}\right)^T * \boldsymbol{K}_{(1,1)}^{DKGQ} * \boldsymbol{K}_{(1,2)}^{DKGQ} \\ &+\&\left(\boldsymbol{K}_{(2,1)}^{DKGQ}\right)^T * \boldsymbol{K}_{(1,1)}^{DKGQ} * \boldsymbol{K}_{(2,1)}^{DKGQ} \\ &+\&\left(\boldsymbol{K}_{(2,2)}^{DKGQ}\right)^T * \boldsymbol{K}_{(1,1)}^{DKGQ} * \boldsymbol{K}_{(2,2)}^{DKGQ} \\ &= \& \begin{bmatrix} k_{11a} & \cdots & k_{11b} \\ \vdots & \ddots & \vdots \\ k_{11c} & \cdots & k_{11d} \end{bmatrix} \end{aligned}$$

$$k_{11a} = k_{(1,1)}^{DKGQ_{(1,1)}} + k_{(1,1)}^{DBC_{(1,1)}}$$

$$k_{11b} = k_{(1,24)}^{DKGQ_{(1,1)}} + k_{(1,1)}^{DKGQ_{(1,2)}}$$

$$k_{11c} = k_{(24,1)}^{DKGQ_{(1,1)}} + k_{(24,1)}^{DBC_{(1,1)}} + k_{(1,1)}^{DKGQ_{(2,1)}}$$

$$k_{11d} = k_{(24,24)}^{DKGQ_{(1,1)}} + k_{(24,1)}^{DKGQ_{(1,2)}} + k_{(1,24)}^{DKGQ_{(2,1)}} + k_{(1,1)}^{DKGQ_{(2,2)}}$$

$$\boldsymbol{K}_{1j} = \&\left(\boldsymbol{K}_{(1,j-1)}^{DKGQ}\right)^{T} * \boldsymbol{K}_{(1,j)}^{DKGQ} * \boldsymbol{K}_{(1,j-1)}^{DKGQ} + \&\left(\boldsymbol{K}_{(2,j-1)}^{DKGQ}\right)^{T} * \boldsymbol{K}_{(1,j)}^{DKGQ} * \boldsymbol{K}_{(2,j-1)}^{DKGQ} + \&\left(\boldsymbol{K}_{(2,j)}^{DKGQ}\right)^{T} * \boldsymbol{K}_{(1,j)}^{DKGQ} * \boldsymbol{K}_{(2,j)}^{DKGQ} + \&\left(\boldsymbol{K}_{(2,j+1)}^{DKGQ}\right)^{T} * \boldsymbol{K}_{(1,j)}^{DKGQ} * \boldsymbol{K}_{(2,j+1)}^{DKGQ} + \&\left(\boldsymbol{K}_{(1,j+1)}^{DKGQ}\right)^{T} * \boldsymbol{K}_{(1,j)}^{DKGQ} * \boldsymbol{K}_{(1,j+1)}^{DKGQ} = \& \begin{bmatrix} k_{1ja} & \cdots & k_{1jb} \\ \vdots & \ddots & \vdots \\ k_{1jc} & \cdots & k_{1jd} \end{bmatrix}$$

$$k_{1ja} = k_{(1,1)}^{DKGQ_{(1,j)}} + k_{(1,24)}^{DKGQ_{(1,j-1)}}$$

$$k_{1jb} = k_{(1,1)}^{DKGQ_{(1,1)}} + k_{(1,1)}^{DKGQ_{(1,2)}}$$

$$k_{1jc} = k_{(24,1)}^{DKGQ_{(1,j)}} + k_{(24,24)}^{DKGQ_{(1,j-1)}} + k_{(1,24)}^{DKGQ_{(2,j-1)}} + k_{(1,1)}^{DKGQ_{(2,j)}}$$

$$k_{1jd} = k_{(24,24)}^{DKGQ_{(1,j)}} + k_{(1,24)}^{DKGQ_{(1,j+1)}} + k_{(1,1)}^{DKGQ_{(2,j+1)}} + k_{(1,24)}^{DKGQ_{(2,j)}}$$

$$\boldsymbol{K}_{1n} = \&\left(\boldsymbol{K}_{(1,2)}^{DBC}\right)^{T} * \boldsymbol{K}_{(1,n)}^{DKGQ} * \boldsymbol{K}_{(1,2)}^{DBC} + \&\left(\boldsymbol{K}_{(1,n-1)}^{DKGQ}\right)^{T} * \boldsymbol{K}_{(1,n)}^{DKGQ} * \boldsymbol{K}_{(1,n-1)}^{DKGQ} + \&\left(\boldsymbol{K}_{(2,n)}^{DKGQ}\right)^{T} * \boldsymbol{K}_{(1,n)}^{DKGQ} * \boldsymbol{K}_{(2,n)}^{DKGQ} + \&\left(\boldsymbol{K}_{(2,n-1)}^{DKGQ}\right)^{T} * \boldsymbol{K}_{(1,n)}^{DKGQ} * \boldsymbol{K}_{(2,n-1)}^{DKGQ} = \& \begin{bmatrix} k_{1na} & \cdots & k_{1nb} \\ \vdots & \ddots & \vdots \\ k_{1nc} & \cdots & k_{1nd} \end{bmatrix}$$

$$k_{1na} = k_{(1,1)}^{DKGQ_{(1,n)}} + k_{(1,24)}^{DKGQ_{(1,n-1)}}$$

$$k_{1nb} = k_{(1,24)}^{DKGQ_{(1,n)}} + k_{(1,1)}^{DBC_{(1,2)}}$$

$$k_{11c} = k_{(24,1)}^{DKGQ_{(1,n)}} + k_{(24,24)}^{DKGQ_{(1,n-1)}} + k_{(1,24)}^{DKGQ_{(2,n-1)}} + k_{(1,1)}^{DKGQ_{(2,n)}}$$

$$k_{11d} = k_{(24,24)}^{DKGQ_{(1,n)}} + k_{(24,24)}^{DBC_{(1,2)}} + k_{(1,24)}^{DKGQ_{(2,n)}}$$

$$\boldsymbol{K}_{ij} = \&\left(\boldsymbol{K}_{(i,j-1)}^{DKGQ}\right)^{T} * \boldsymbol{K}_{(i,j)}^{DKGQ} * \boldsymbol{K}_{(i,j-1)}^{DKGQ} + \&\left(\boldsymbol{K}_{(i,j+1)}^{DKGQ}\right)^{T} * \boldsymbol{K}_{(i,j)}^{DKGQ} * \boldsymbol{K}_{(i,j+1)}^{DKGQ} + \&\left(\boldsymbol{K}_{(i+1,j)}^{DKGQ}\right)^{T} * \boldsymbol{K}_{(i,j)}^{DKGQ} * \boldsymbol{K}_{(i+1,j)}^{DKGQ} + \&\left(\boldsymbol{K}_{(i-1,j)}^{DKGQ}\right)^{T} * \boldsymbol{K}_{(i,j)}^{DKGQ} * \boldsymbol{K}_{(i-1,j)}^{DKGQ} + \&\left(\boldsymbol{K}_{(i+1,j-1)}^{DKGQ}\right)^{T} * \boldsymbol{K}_{(i,j)}^{DKGQ} * \boldsymbol{K}_{(i+1,j-1)}^{DKGQ} + \&\left(\boldsymbol{K}_{(i+1,j+1)}^{DKGQ}\right)^{T} * \boldsymbol{K}_{(i,j)}^{DKGQ} * \boldsymbol{K}_{(i+1,j+1)}^{DKGQ} + \&\left(\boldsymbol{K}_{(i-1,j-1)}^{DKGQ}\right)^{T} * \boldsymbol{K}_{(i,j)}^{DKGQ} * \boldsymbol{K}_{(i-1,j-1)}^{DKGQ} + \&\left(\boldsymbol{K}_{(i-1,j+1)}^{DKGQ}\right)^{T} * \boldsymbol{K}_{(i,j)}^{DKGQ} * \boldsymbol{K}_{(i-1,j+1)}^{DKGQ} = \& \begin{bmatrix} k_{ija} & \cdots & k_{ijb} \\ \vdots & \ddots & \vdots \\ k_{ijc} & \cdots & k_{ijd} \end{bmatrix}$$

$$k_{ija} = k_{(1,1)}^{DKGQ_{(i,j)}} + k_{(24,1)}^{DKGQ_{(i-1,j)}} + k_{(24,24)}^{DKGQ_{(i-1,j-1)}} + k_{(1,24)}^{DKGQ_{(i,j-1)}}$$

$$k_{ijb} = k_{(1,24)}^{DKGQ_{(i,j)}} + k_{(24,24)}^{DKGQ_{(i-1,j)}} + k_{(24,1)}^{DKGQ_{(i-1,j+1)}} + k_{(1,1)}^{DKGQ_{(i,j+1)}}$$

$$k_{ijc} = k_{(24,1)}^{DKGQ_{(i,j)}} + k_{(24,24)}^{DKGQ_{(i,j-1)}} + k_{(1,24)}^{DKGQ_{(i+1,j-1)}} + k_{(1,1)}^{DKGQ_{(i+1,j)}}$$

$$k_{ijd} = k_{(24,24)}^{DKGQ_{(i,j)}} + k_{(24,1)}^{DKGQ_{(i,j+1)}} + k_{(1,1)}^{DKGQ_{(i+1,j+1)}} + k_{(1,24)}^{DKGQ_{(i+1,j)}}$$

The calculation methods for the rest of the positions are similar to the above method.

2.5. Validation of linear elastic model

To verify the theoretical accuracy of the double vertical beam shell model, a simple model of the double vertical beam shell unit was set up as shown in Fig. 2. Using a fully linear elastic material, the characteristic values were calculated and compared with the results of material mechanics calculations.

The model shown in Fig. 2 is composed of a shell element DKGQ in the middle and a nonlinear beam-column part on the left and right sides. It is the simplest form of DVBSE, where the nonlinear beam-column is bound to the master node with the plane shell element. In actual simulations, there are often multiple shell elements connected in the middle of DVBSE. To facilitate numerical analysis, all quantities in this model were not specified in units, and the default unit was 1. The width of the plane shell element DKGQ was 1 and the thickness was 0.25; the length of the two nodes of the nonlinear beam-column part was the same as the height of the plane shell element DKGQ, and the cross-section was a square of 0.25×0.25; all elements used linear elastic material $E = 1.0 \times 10^{10}$, $\mu = 0.25$; a force of $F = 1.0 \times 10^{5}$ was applied at node 1. Nodes 2 and 4 were fully constrained.

According to the specification, it is divided into three cases: high walls with a height-width ratio greater than 2 (h/b > 2), medium-high walls with a height-width ratio less than 2 but greater than 1 (1 < h/b < 2), and low walls with a height-width ratio less than 1 (h/b < 1). The heights were set as follows: 2 and 3 for high walls, 1 and 1.5 for medium-high walls, and 0.8 for low walls. The displacement of node 2 along the loading direction was calculated using both the material mechanics method and the finite element method of the double vertical beam shell unit. The results are shown in Table 2.

Table 2 reveals that the displacement predicted by the FE model is usually larger than that obtained by the mechanics of materials. This may be due to the limited number of finite element nodes, leading to a slightly larger overall stiffness. The performance of this simple model is excellent for high and low wall cases but is more general for medium-high wall cases. High walls are primarily affected by bending moments, while low walls are primarily affected by shear, and the force conditions are relatively simple. When the simple model is applied to high and low walls, the results are consistent, indicating the robust performance of the DVBSE in a single force state. When the simple model is applied to medium-high walls, the error is slightly larger than for high and low walls but remains within a reasonable range. One of contributing factors is that when the aspect ratio is relatively small, the number of beam-column nodes is small, resulting in a stiff performance, while the plane shell elements are not sufficiently flexible. Another factor is that in the simple model, the proportion of beam-columns is 2:1, which closely simulates the beam-columns.

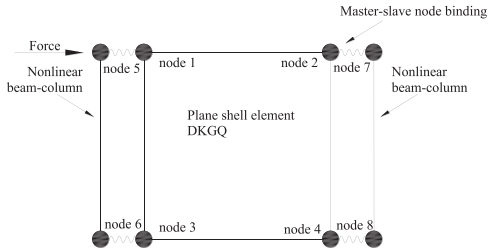

Fig. 2. The simplest model of the double vertical beam shell.

Table 1
Basic data of the simplest double vertical beam shell model.

Width	Thickness	Cross-section	Material type	Rigidity	Poisson's ratio	Force
1	0.25	0.25 × 0.25	linear-elastic material	$1.0 * 10^{10}$	0.25	$1.0 * 10^{5}$

Table 2
Comparison of theoretical results.

Shear wall type	Height-width ratio	Finite element solution	Material mechanics theoretical solution	Error
High wall	3	0. 25994	0.26466	1%
High wall	2	0. 15179	0.14976	1%
Medium-high wall	1.5	0.02933	0.02975	2%
Medium-high wall	1	0.01186	0.01216	3%
Low wall	0.8	$1.11 * 10^{-6}$	$1.13 * 10^{-6}$	1%

3. Implementation of DVBSE in OpenSees

3.1. Implementation procedure

OpenSees, an open-source software, fosters a collaborative environment where users and researchers can write code to utilize and develop the platform. This approach enhances the public's potential for code research, allowing researchers to collaborate freely across time and space, using code as a medium for communication [25]. In this context, the user script side is referred to as the front-end, while the developer side is referred to as the back-end. This research has leveraged the advantages of OpenSees platform to develop a new shear wall element to ensure flexibility and reusability of the DVBSE program.

The OpenSees program employs an object-oriented design methodology, which initially identifies abstract components required in the finite element analysis, such as materials, nodes, elements, and algorithms. These components are encapsulated into distinct base classes, including node, material, and element base classes, among others. Subsequently, derived subclasses are implemented from the base classes to address specific engineering problems. For instance, the Steel02 material subclass was derived from the uniaxialMaterial parent class, significantly enhancing the reusability of the program. The calculations for transverse and longitudinal reinforcement are performed based on the volume and spacing of the steel bars.

The implementation steps of the double vertical beam-shell element in OpenSees are shown in Fig. 3 and described as follows:

(1) Determine the front-end script call method for the DVBSE.
(2) Write the source code and implement a subclass within the Element abstract base class.
(3) Add element information by modifying the classTag.h file to assign a unique identifier to the element, enabling recognition by other parts of OpenSees.
(4) Ensure the front-end script's DVBSE specification is recognized by creating a new modeling command for the element in the TclModelBuilderElementCommand() function within TclElementCommands.cpp.
(5) Add the path and compile the entire program.

3.2. DVBSE front-end script call

To build a model for the new shear wall, only two points and at least two sections are needed. Simultaneously, the front-end script should consider both calculation efficiency and calculation accuracy. DVBSE consists of three major modules: domain, analysis, and recorder, as illustrated in Fig. 4. The Recorder module includes effective recorder items for DVBSE, such as global force (including forces, globalForce), local force (including localForce and localForces), lateral displacement magnitude (including basicStiffness), stiffness matrix output (including chordRotation, chordDeformation, basicDeformation), and section displacement and force (including sectionDisplacements, sectionForces). Through these external interfaces, DVBSE can effectively communicate key information within the OpenSees framework via scripts.

To determine the basic geometric information of the shear wall, only two user-defined nodes are required. The modeling process is completed by specifying grid density, with $vertical_number indicating the vertical grid density and $middleNumber representing the horizontal grid density. During the modeling process, the program compares the difference in height between the two center points of the unit and the shear wall's height to prevent errors. The program automatically creates calculation nodes when forming the units, significantly enhancing computational efficiency without sacrificing accuracy.

DVBSE necessitates two sections for the unification of edge-constrained components in the shear wall: the LayeredShell section for simulating the shear wall web area and the Fiber section for simulating the constraint edge components. To avoid errors such as inconsistent thickness between the shear wall transfer thickness and the central shell section thickness in the equivalent beam model of the edge region, it is

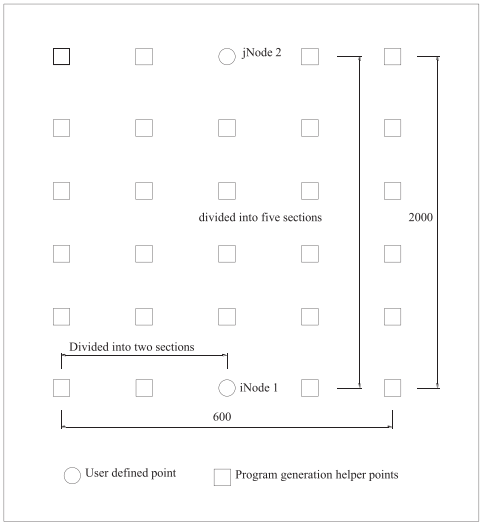

Fig. 4. Modeling of DVBSE.

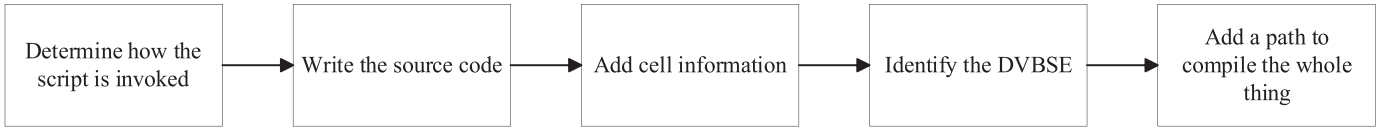

Fig. 3. Implementation steps of double vertical beam-shell element in OpenSees.

essential to compare and verify the corresponding regions.

3.3. DVBSE back-end integration

The computer flowchart of the DVBSE model is shown in Fig. 5 and 6.

During the calculation process of DVBSE, the units are first initialized and checked, while nodes, loads, and stiffness matrices are implemented. Subsequently, the local coordinate system is established, and the stiffness matrix in the global coordinate system is obtained through the calculation program. The back-end code consists of DVBSE.h and DVBSE.cpp, which describe the main functions of the DVBSE class, as well as the relationships between various functions and functional modules. After writing the back-end code, a function is required to link the front and back ends. OpenSees prioritizes this function existing in DVBSE.cpp, and it is conventionally named OPS_DVBSE. This function is responsible for checking and passing parameters and initializing the DVBSE unit class. Finally, within TclElementCommands.cpp's TclModelBuilderElementCommand() function, a branch is created for the unit, which calls the OPS_DVBSE.

It is important to note that when a new unit is added, the virtual functions in the Element abstract base class must be implemented. Therefore, the developer's new unit must inherit the Element abstract base class.

3.4. The compilation process

The most basic compilation process for OpenSees necessitates the support from the script library and the Intel Fortran compiler. However, the design of the LayeredShell section also requires the support from the Intel MKL library. It is essential to note that when configuring the Visual Studio environment, the compilation mode should be selected as Release, in x64 mode. Additionally, Tcl and Python header file addresses and static link library addresses must be added. The compilation process involving all libraries is given as follows:

(1) OpenSees source code.
(2) Visual Studio.
(3) Support from the following libraries and compiler:

Git distributed management system.
Script runtime libraries.
Intel Fortran compiler.
Intel MKL Arithmetic library.

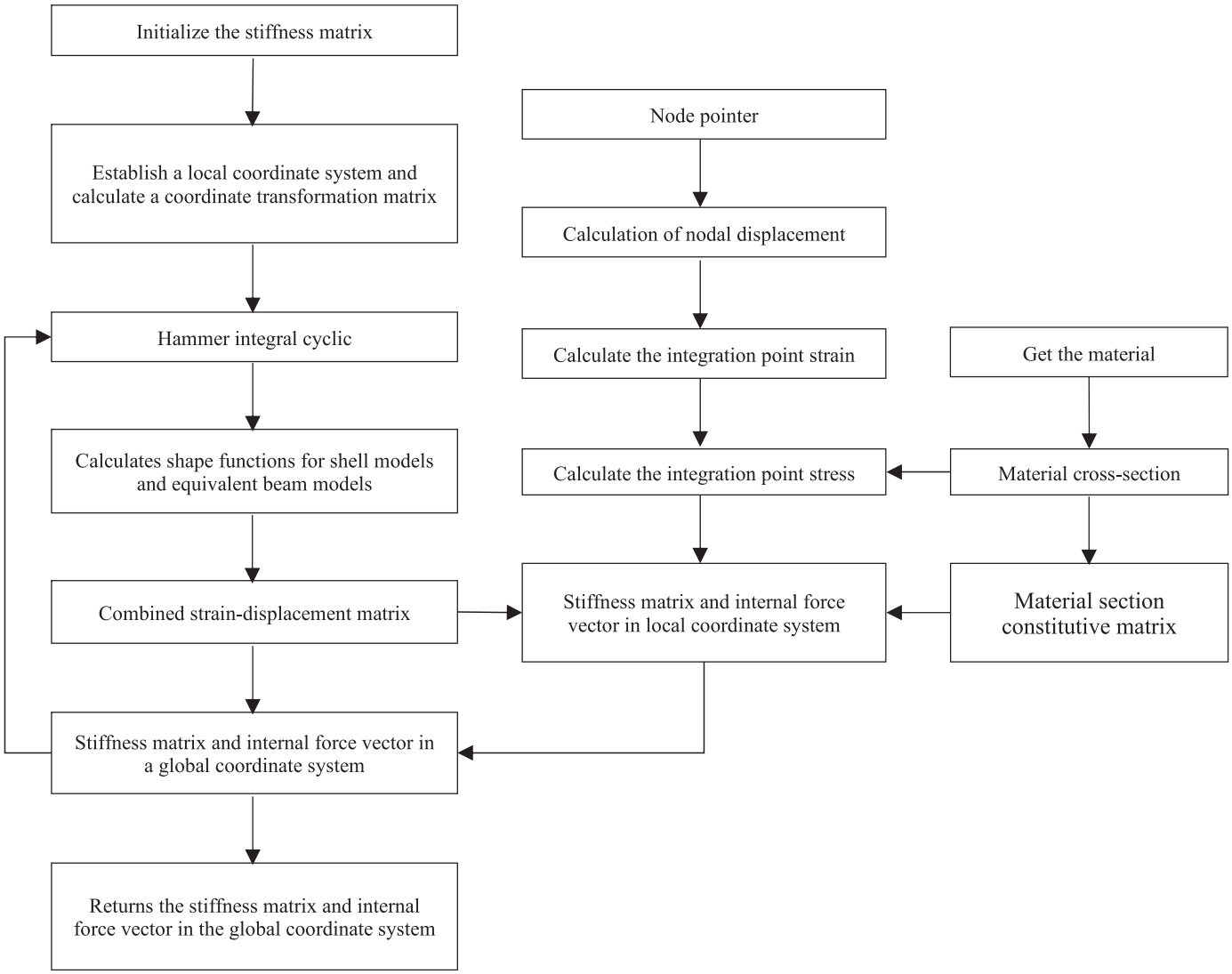

Fig. 5. The computer flowchart of the DVBSE model.

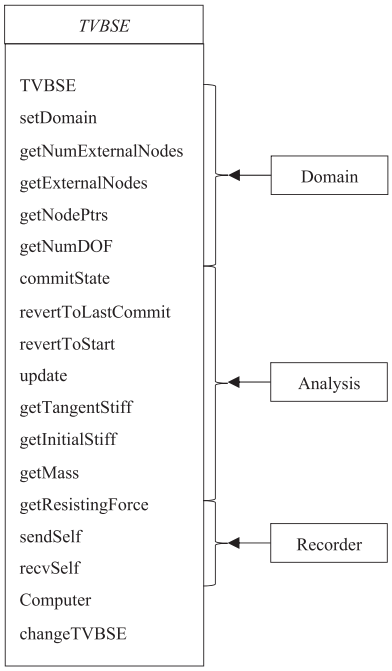

Fig. 6. The architecture of DVBSE.

4. Verification of the developed shear wall element

4.1. Description of tested shear wall

To verify the reliability of DVBSE in simulating complex shear walls, the SW01 and the SW04 shear walls tested by our research group were selected. These new shear walls were made of C40 sea sand concrete, and the main reinforcing steel in the constrained edge members consisted of steel-continuous fiber composite reinforcement. The edge region incorporated GFRP reinforcement to provide self-recovery ability. The self-centering shear wall uses steel-fiber reinforcements to absorb energy and minimize deformation. GFRP's strength prevents yielding, promoting resilience and reducing residual deformation. The tested shear walls are depicted in Fig. 7. The test setup is shown in Fig. 8.

The end longitudinal bars were composed of S16G2 composite bars with a diameter of 20 mm, while the longitudinal distribution bars in the wall were selected as S6G2 composite bars with a diameter of 10 mm.

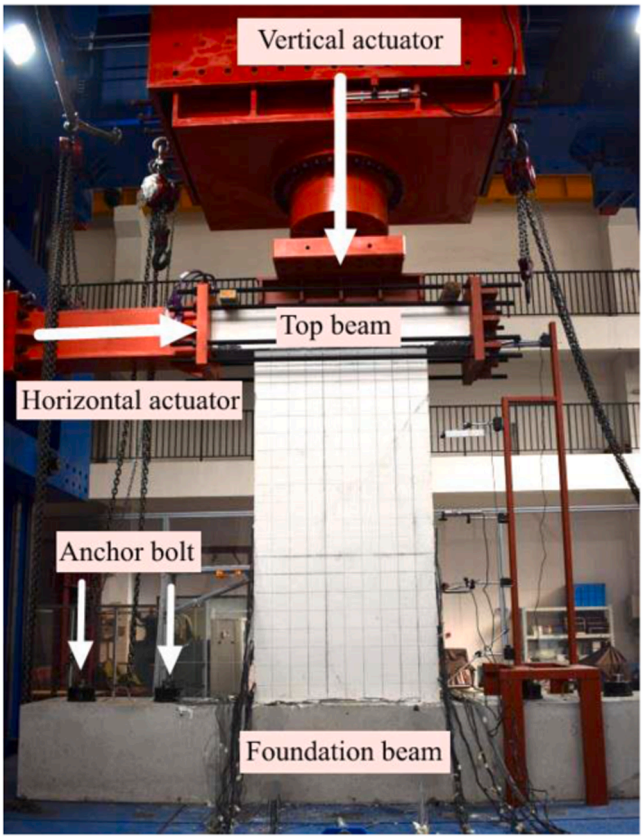

Fig. 8. Test Setup.

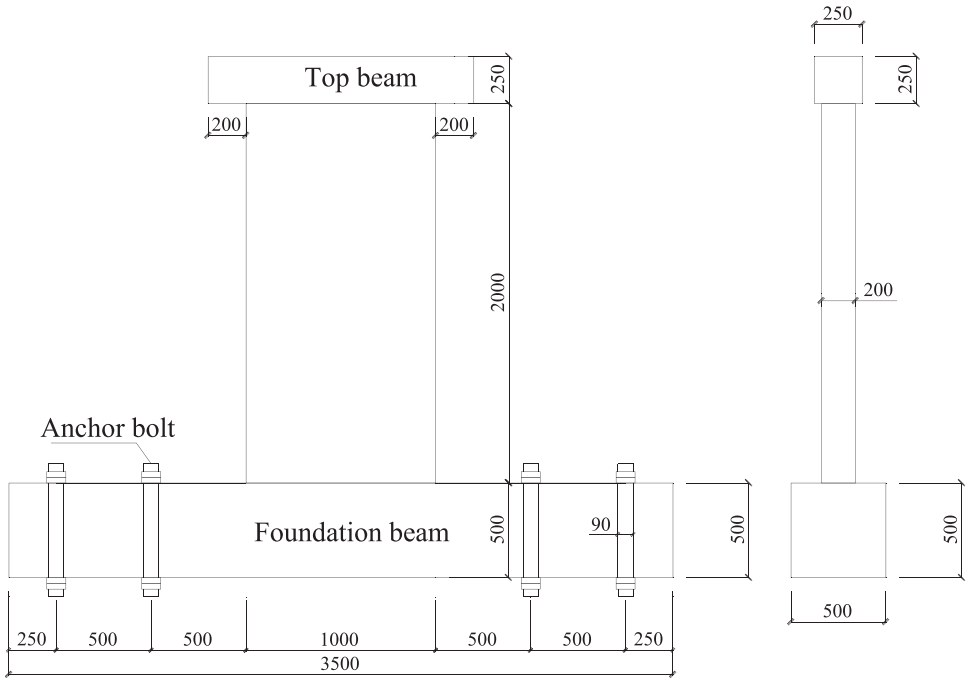

Fig. 7. Specimen Dimension.

The lateral ties were made of GFRP bars with a diameter of 8 mm.

The shear reinforcement details for the wall steel are listed in Table 4 and Fig. 9. To validate the reliability of the DVBSE method, two specimens, SW01 and SW04, were subjected to simulation testing. The information for the two shear walls is presented in Table 3.

In the experiment, the end GFRP (Glass Fiber Reinforced Polymer) longitudinal bars, with a diameter of 20 mm, were employed, along with S16G2 transverse bars representing 2-mm thick glass fiber wrapping around HRB400 steel bars of 16-mm diameter as composite reinforcement. Stirrups and intermediate longitudinal bars were represented by S6G2, denoting 2-mm thick glass fiber wrapping around HRB400 steel bars of 6-mm diameter as composite reinforcement. The specific strength information is detailed in Table 4. It is important to note that GFRP bars lack a yield plateau and behave linearly until reaching their ultimate strength.

4.2. Material constitutive laws for steel reinforcement

Initially, it is essential to determine the uniaxial materials for steel reinforcement and concrete. In addition, in the shell model, both concrete and hoop reinforcement are subjected to horizontal loads; thus, an additional two-dimensional constitutive material model should be determined.

The constitutive model for steel reinforcement used in this study was Steel02, which accounts for isotropic strain hardening and the Bauschinger effect. It is based on the Menegotto steel reinforcement constitutive model. This model conforms to the consistency of the steel reinforcement reloading test results as shown in Fig. 10.

4.3. Uniaxial constitutive model for concrete

The Concrete01 Material and Concrete02 Material were used as the uniaxial constitutive models for concrete. For concrete materials subjected to earthquake and cyclic loading, it is necessary to define additional hysteretic rules. Concrete01 does not account for the tensile state of concrete and employs linear unloading during the unloading process. Conversely, Concrete02 utilizes piecewise linear unloading.

4.4. Two-dimensional morphable materials

For two-dimensional materials, PlaneStressUserMaterial, PlateRebar, and PlateFromPlaneStress proposed by Lu et al. [26], were used to model the central shell of the shear wall. The steps are as follows:

Construction of plane stress multi-dimensional material:

(*nDmaterial PlaneStressUserMaterial*) .

Construction of concrete plane stress material:

(*nDmaterial PlaneStressUserMaterial $matTag 40 7 $fc $ft $fcu $epsc0 $epscu $epstu $st-c*) .

Where f_c is the 28-day compressive strength of the concrete, f_t is the tensile strength of the concrete, f_{cu} is the residual strength of the concrete, *epsc*0 is the maximum compressive strain of the concrete, *epscu* is the residual compressive strain of the concrete, *stc* is the shear strength retention factor.

Assign shear stiffness to the plane to form a multi-dimensional material of the layered shell concrete layer:

(*nDmaterial PlateFromPlaneStress $newmatTag $matTag $OutofPlaneModulus*) .

The material for concrete plane stress is defined by the matTag and the OutofPlaneModulus. The Steel02 material can be employed to construct a multi-dimensional steel reinforcement layer (nDmaterial PlateRebar) for a layered shell grid. The command for this is (nDmaterial PlateRebar $newmatTag $matTag $sita), where matTag refers to the material for uniaxial steel reinforcement, and sita represents the angle of the steel reinforcement. For longitudinal reinforcement, the angle is 90, while for transverse reinforcement, the angle is 0.

The material setting is complete.

4.5. Assembled section

Due to the different regions of the DVBSE constraint components on both sides and in the middle, two types of section assembly are required. One is the Fiber section (simulating the region of constraint components on both sides), and the other is the LayeredShell section (simulating the central region).

Fiber section:

(*section Fiber $secTag -GJ $GJ* { *fiber1 fiber2* …}).

To prevent twisting strains from causing non-convergence, the linear elastic torsional stiffness Gj assigned to this part can be adjusted to a maximum value, such as 10^{14}.

LayeredShell section:

(*section LayeredShell $sectionTag $nLayers $matTag1 $thickness1. $matTagn $thickness-n*).

Here, *nLayers* represents the total number of section shell layers, *matTag* refers to the multi-dimensional material number, and thickness denotes the equivalent volume thickness.

To pass the geometric transformation object to the equivalent constraint edge component region on both sides:

(*geomTransf Linear $transfTag $vecxzX $vecxzY $vecxzZ*).

In this command, *transfTag* represents the number of the local coordinate axis vector, while *vecxzX*, *vecxzY*, and *vecxzZ* identify the direction vector of the local coordinate axis (projecting the local z-axis on the left onto the global coordinate system).

4.6. Loading method

Following the same approach as the experimental loading method, the quasi-static loading method and displacement control loading mode were employed. The total displacement length was 72 mm, with 19 hysteresis cycles being loaded, and the increment for each cycle was 4 mm. Measurements were recorded once every 2-mm increment.

4.7. Results and discussion

The predicted cyclic load-displacement curves of the shear wall by using DVBSE are compared with experimental data in Fig. 11, revealing a notable agreement between simulation and experimental data. The hysteresis curves shown in Fig. 11 represent restoring force characteristic curves. As depicted in Fig. 11(a), the rising branch of the hysteresis curve exhibits better consistency than the descending branch. After passing the peak point, the simulation curve drops faster than the experimental one. This divergence may be attributed to defects and artificial damage in the shear wall before and during the installation, and a small amount of slip between concrete and steel bars in the shear wall. It's important to note that the computer simulation was run in an ideal state without additional errors.

The skeleton curve connects the extreme points of each loading in the

Table 3
Shear Wall Information.

Specimen	Height-width ratio	Axial load ratio	Diameter of End GFRP reinforcement	Stirrup spacing	End longitudinal reinforcement	Wall reinforcement with hoop reinforcement
SW01	2.125	0.2	20	40	S16G2	S6G2
SW04	2.125	0.3	26	80	S16G2	S6G2

Table 4
Shear wall bar material strength.

Specification	Inner core steel bar diameter (mm)	Fiber layer thickness (mm)	Diameter (mm)	Yield strength (N/mm^2)	Ultimate strength (N/mm^2)	Yield strain (%)	Ultimate strain (%)
GFRP	–	–	20	–	1255.5	–	1.980
S16G2	16	2	20	348.7	718.4	0.204	1.923
S6G2	6	2	10	257.5	837.2	0.196	1.658

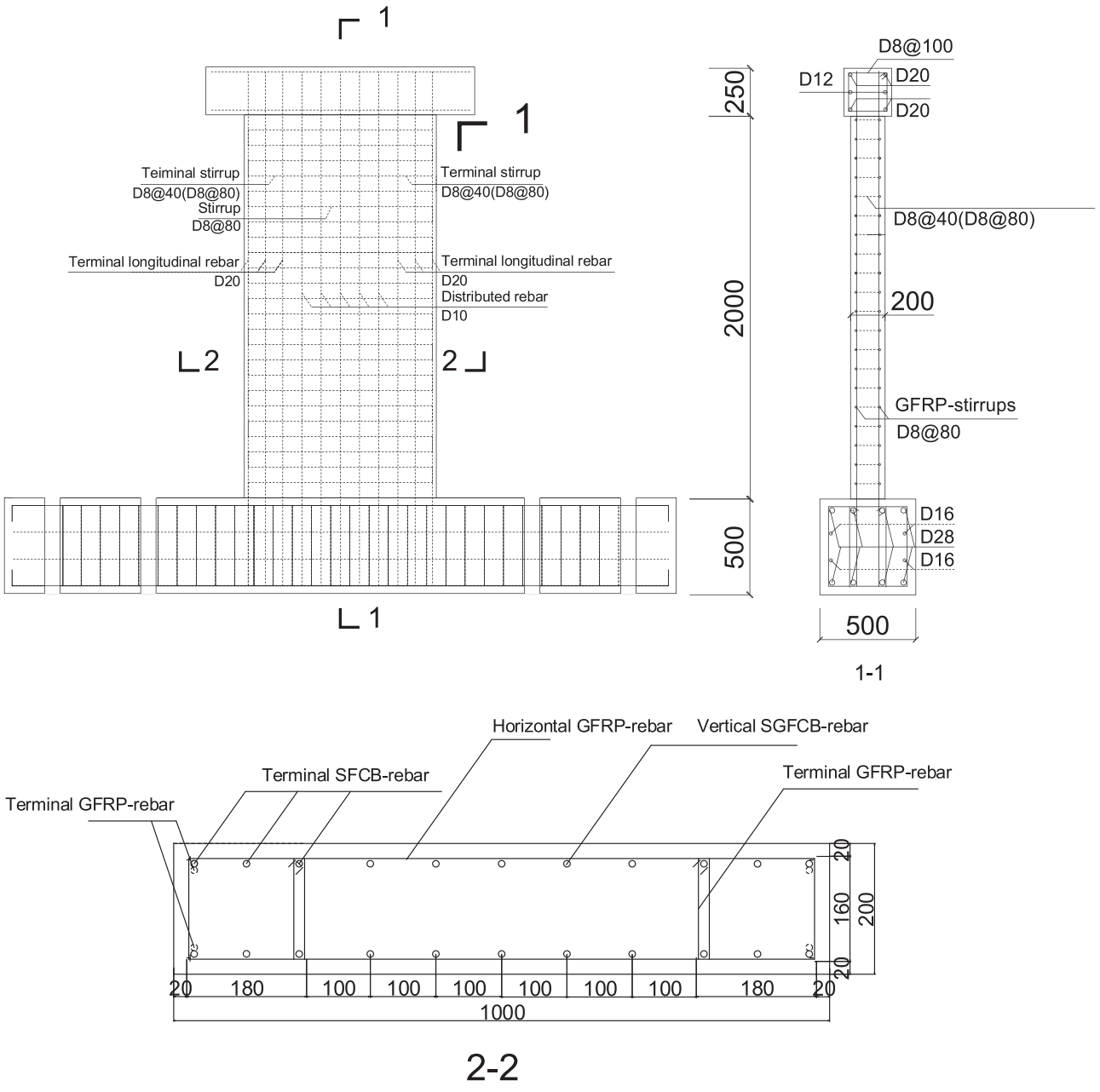

Fig. 9. Reinforcement details of shear wall.

same direction in the hysteresis curve. As shown in Fig. 11(b), in the skeleton curve, the consistency of each characteristic point in each stage is good, and the overall consistent trend indicates that the DVBSE yields accurate simulation of the responses of shear wall.

Stiffness degradation refers to the phenomenon that the stiffness decreases continuously in the process of continuous accumulation of damage in the shear wall. As shown in Fig. 11(c), in the early stages of loading, the experimental curve has a phenomenon slightly lower than the simulation curve, potentially due to experiment instability and more external interference factors.

The single cycle energy dissipation curve reflects the energy consumption of the material during the loading process. As shown in the comparison of Fig. 11(d), the overall trend is consistent, but the measured energy consumption is lower than that of the simulation result. This discrepancy arises from the material setting in OpenSees used ordinary concrete and ordinary steel bars, while the seawater sand

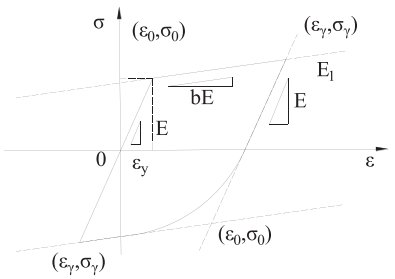

Fig. 10. Constitutive model of Steel02.

concrete and composite bars were used to construct the shear wall specimen. Consequently, the this led to deviation in energy consumption.

In summary, the predicted cyclic load-displacement curves for the tested shear wall are generally in good agreement with experimentally measured data, which reflects high degree of accuracy of DVBSE proposed in this paper. Although there are uncontrollable factors in the experiment, the differences between simulation and experiment are minimal and traceable. Therefore, the proposed DVBSE has high reliability in the numerical calculation of complex shear walls.

In order to validate the rationality and reusability of DVBSE, another experimental component SW04 tested by our research group is selected for verification. The shear wall information is listed in Table 3.

The difference from the previous example lies in the axial compression ratio changing from 0.2 to 0.3, the end GFRP bar diameter increasing from 20 mm to 26 mm, and the spacing between stirrups changing from 40 mm to 80 mm (resulting in a halving of stirrup density). All other parameters remain unchanged, including materials, cross-sections, and loading conditions, thus only involving modifications in three parameters. Therefore, the material settings, section assembly, and loading method mentioned earlier all remain the same.

The simulation results using Opensees are shown in Fig. 12. The figure demonstrates that the agreement between the experimental and DVBSE-simulated hysteresis curves is excellent. The forward loading curve exhibits a slightly higher conformity compared to the reverse loading curve, demonstrating the continued precision and strong reusability of DVBSE. The overall trend closely matches the skeleton curve of SW04. The stiffness degradation curve also closely resembles the experimental curve, with only minor discrepancies within a displacement of 10 mm. In the single loop energy dissipation curve, the simulation results of DVBSE remain.

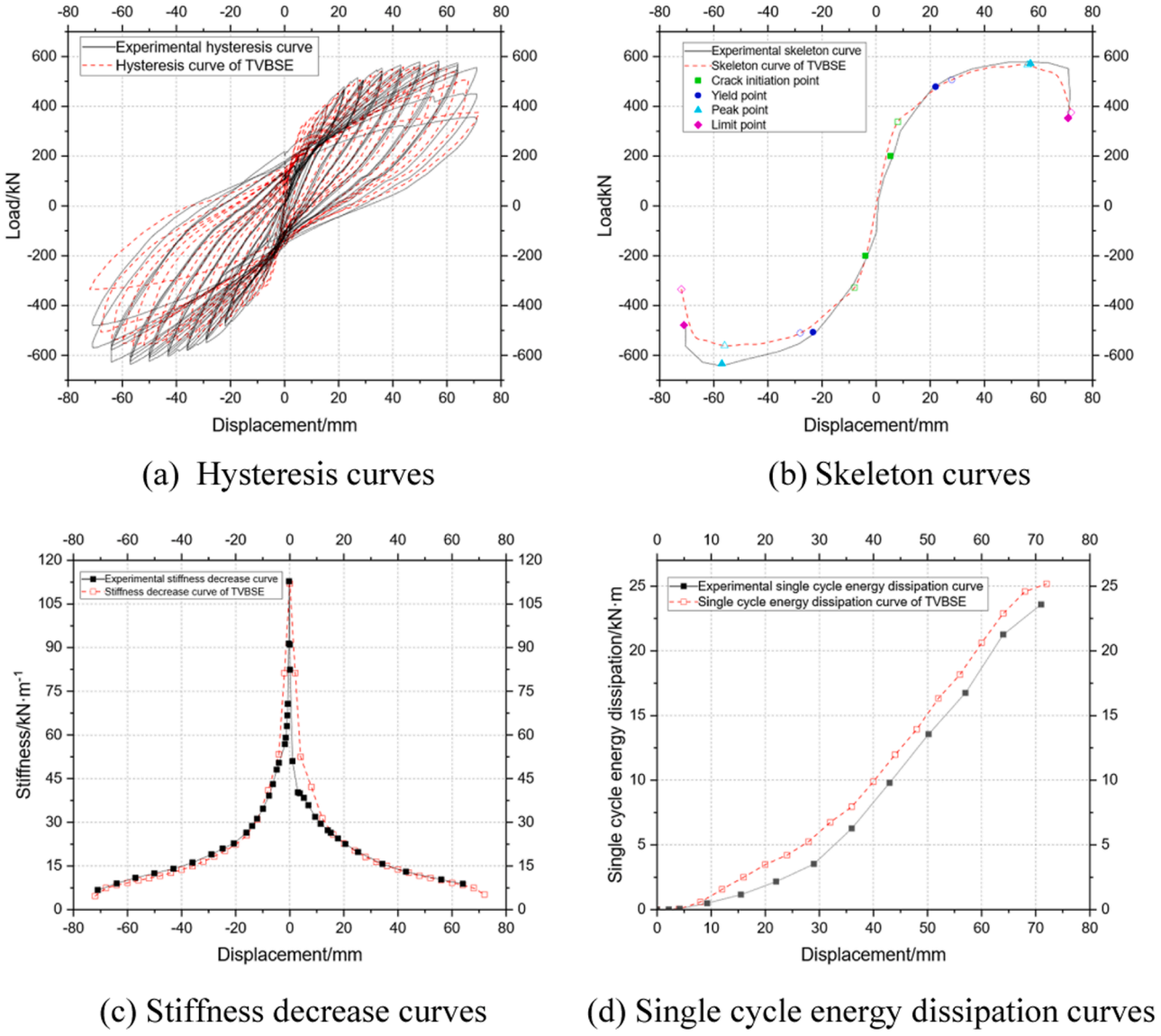

Fig. 11. Comparison of predictions by DVBSE and experimental results.

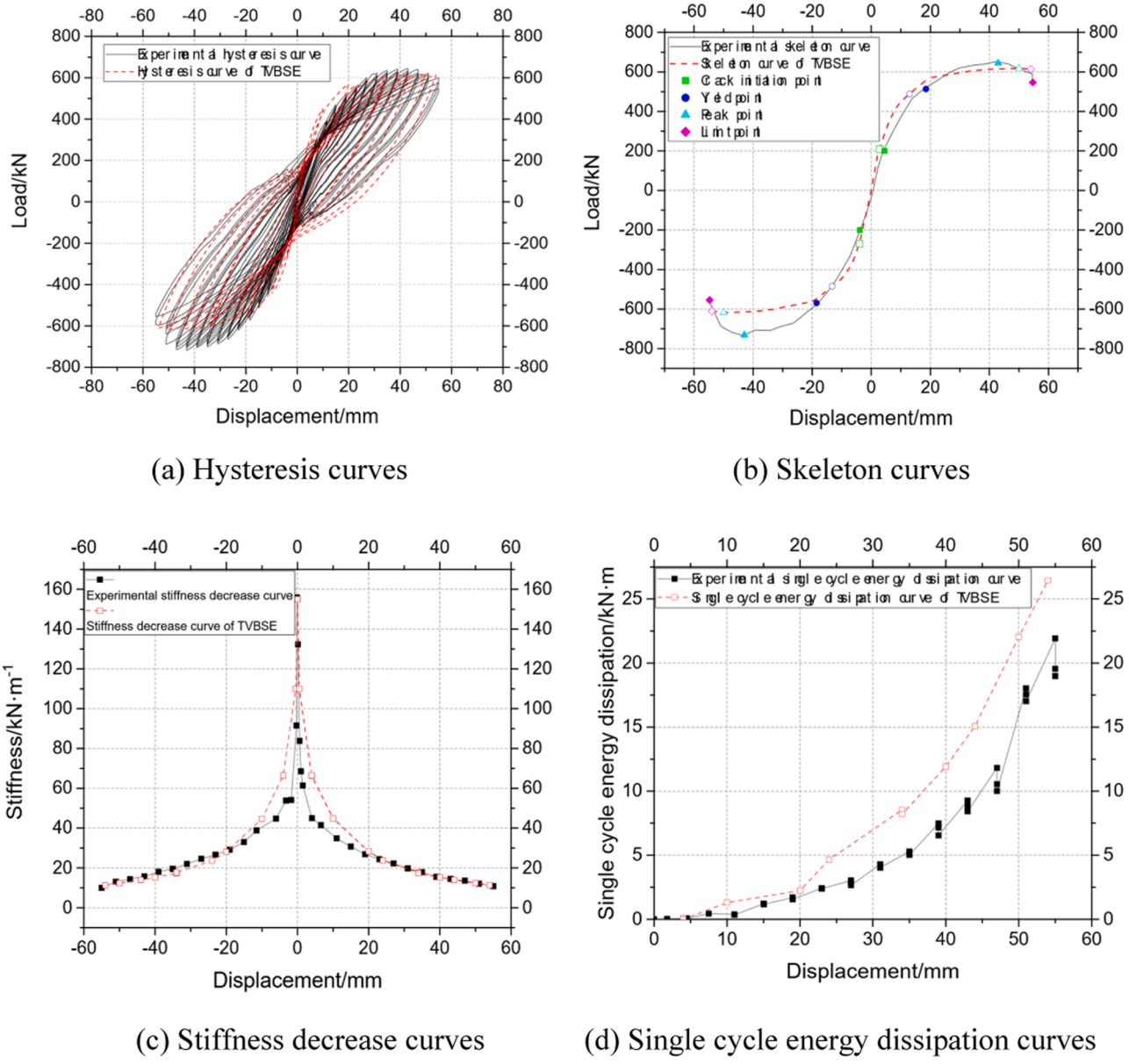

Fig. 12. Comparison of computational and experimental results of shear wall SW04.

slightly higher than the experimental curve. This is attributed to the material loss and human errors inherent in the experiment, while the computer simulation assumed ideal conditions. Thus, a higher energy dissipation curve is reasonable in this context.

In conclusion, the simulated curves of DVBSE closely match the experimental results, highlighting the high simulation accuracy and strong reusability of DVBSE. Furthermore, the minor discrepancies between the experimental and simulated curves stem from potential variations in the testing environment and human manipulation, which are typical within reasonable bounds.

5. Conclusions

In this paper, a novel finite element, referred to as the Double Vertical Beam-column with Shell Element (DVBSE), has been developed and presented for simulating the responses of complex shear walls subjected to seismic loads. The DVBSE has been implemented in the OpenSees program. The accuracy of the DVBSE was rigorously assessed by comparing finite element simulations with the experimental results of self-centering shear walls composed of steel-GFRP composite bars and sea sand concrete. The following conclusions can be drawn from this study:

(1) The newly developed DVBSE makes a significant advancement in the simulation of complex shear walls and its innovation lies in integrating the edge members and shear wall plate into one element which accurately simulates complex structures, enhancing the reliability and adaptability of shear wall simulations. A good agreement between the simulated hysteresis curve and experimental results validates the effectiveness of the DVBSE in capturing the behavior of innovative shear walls.

(2) High-performance quadrilateral plate elements, specifically the NLDKGQ, are utilized in the core regions of shear walls, while equivalent fiber beam models are employed in the edge areas. A good agreement between the simulated hysteresis curve and experimental results validates the effectiveness of the DVBSE in capturing the behavior of innovative shear walls.

(3) The theoretical feasibility of DVBSE is substantiated through comprehensive theoretical analysis and rigorous formula derivation. The analysis of DVBSE is predicated upon its distinctive configuration with particular emphasis on three integral aspects: boundary constraint handling, external load processing, and stiffness matrix formulation. Specifically, boundary constraint handling is facilitated through the implementation of master-slave nodes; external load processing was achieved by employing rigid beams at the apex; and Eq. (10) delineates the global stiffness matrix intrinsic to DVBSE.
(4) The integration steps and specific implementation process of DVBSE within the OpenSees framework have been meticulously delineated. Due to the open-source nature of OpenSees, the DVBSE developed in this study exhibits a high degree of flexibility and reusability. Two distinct specifications of innovative complex shear walls were selected for simulation, with both results proving highly satisfactory and thus demonstrating the substantial reusability of the DVBSE methodology.
(5) This research advances a systematic methodology for simulating the behavior of complex shear walls, with a specific focus on seismic performance of recoverable structures. It should be noted that the DVBSE proposed in this paper has only been employed for simulating reinforced concrete shear walls. Future research should be conducted to extend its application to steel plate shear walls and steel-concrete composite shear walls.

CRediT authorship contribution statement

Xiru Hang: Writing – original draft, Visualization, Software. **Minsheng Guan:** Writing – review & editing, Methodology, Funding acquisition, Conceptualization. **Mengsen Wang:** Software, Investigation, Formal analysis. **Qing Quan Liang:** Writing – review & editing, Visualization, Supervision. **Hanyuan Zhao:** Validation, Data curation. **Ying Wang:** Methodology.

Declaration of Competing Interest

The authors whose names are listed immediately below certify that they have NO affiliations with or involvement in any organization or entity with any financial interest (such as honoraria; educational grants; participation in speakers' bureaus; membership, employment, consultancies, stock ownership, or other equity interest; and expert testimony or patent-licensing arrangements), or non-financial interest (such as personal or professional relationships, affiliations, knowledge or beliefs) in the subject matter or materials discussed in this manuscript.

Data availability

Data will be made available on request.

Acknowledgments

This research was supported by the National Natural Science Foundation of China (Grant No. 52278195).

References

[1] Villaverde R. Methods to assess the seismic collapse capacity of building structures: state of the art. J Struct Eng, ASCE 2007;133(1):57–66.
[2] Fragiadakis M, Lagaros ND. An overview to structural seismic design optimisation frameworks. Comput Struct 2011;89(11-12):1155–65.
[3] Yang TY, Tung DP, Li YJ. Equivalent energy design procedure for earthquake resilient fused structures. Earthq Spectra 2018;34(2):795–815.
[4] Deng KL, Wang T, Kurata M, Zhao CH, Wang KK. Numerical study on a fully-prefabricated damage-tolerant beam to column connection for an earthquake-resilient frame. Eng Struct 2018;159:320–31.
[5] Rong B, Lu K, Ni XJ, Ge J. Hybrid finite element transfer matrix method and its parallel solution for fast calculation of large-scale structural eigenproblem. Appl Math Model 2020;77:169–81.
[6] Eatherton MR, Ma X, Krawinkler H, Deierlein GG, Hajjar JF. Quasi-Static cyclic behavior of controlled rocking steel frames. J Struct Eng ASCE 2014;140(11): 04014083.
[7] Wu YW, Fan SG, Zhou H, Guo Y, Wu QX, Deierlein G. Cyclic behaviour of diagonally stiffened stainless steel plate shear walls with two-side connections: experiment, simulation and design. Eng Struct 2022;268:114756.
[8] Li XM, Zhang FW, Wang ZL, Tian K, Dong JZ, Jiang L. Shaking table test of a frame structure retrofitted by externally-hung rocking wall with SMA and disc spring self-centering devices. Eng Struct 2021;240:112422.
[9] Dehcheshmeh EM, Broujerdian V. Determination of optimal behavior of self-centering multiple-rocking walls subjected to far-field and near-field ground motions. J Build Eng 2022;45:103509.
[10] Broujerdian V, Dehcheshmeh EM. Locating the rocking section in self-centering bi-rocking walls to achieve the best seismic performance. Bull Earthq Eng 2022;20: 2441–68.
[11] Abualreesh AM, Tuken A, Albidah A, Siddiqui NA. Reliability-based optimization of shear walls in RC shear wall-frame buildings subjected to earthquake loading. Case Stud Constr Mater 2022;16:e00978.
[12] Mohamed N, Farghaly AS, Benmokrane B, Neale KW. Flexure and shear deformation of GFRP-Reinforced shear walls. J Compos Constr 2014;18(2): 04013044.
[13] Sun XF, He MJ, Li Z, Lam F. Seismic performance of energy-dissipating post-tensioned CLT shear wall structures I: shear wall modeling and design procedure. Soil Dyn Earthq Eng 2020;131:106022.
[14] Chang TL, Lee CL, Carr AJ, Dhakal RP. Numerical evaluations of a novel membrane element in simulations of reinforced concrete shear walls. Eng Struct 2019;199: 109592.
[15] Liang QQ. Numerical simulation of high strength circular double-skin concrete-filled steel tubular slender columns. Eng Struct 2018;168:205–17.
[16] Guan MS, Wang X, Heng JL, Sha M, Du HB. Parametric study on lateral behaviour of composite shear walls with high-strength manufactured sand concrete. Structures 2023;49:332–44.
[17] Murano A, Mehrotra A, Ortega J, Rodrigues H, Vasconcelos G. Comparison of different numerical modelling approaches for the assessment of the out-of-plane behaviour of two-leaf stone masonry walls. Eng Struct 2023;291:116466.
[18] Yam MCH, Fang C, Lam ACC, Zhang Y. Numerical study and practical design of beam-to-column connections with shape memory alloys. J Constr Steel Res 2015; 104(10):177–92.
[19] Kolozvari K, Orakcal K, Wallace JW. New OpenSees models for simulating nonlinear flexural and coupled shear-flexural behavior of RC walls and columns. Comput Struct 2017;196:246–62.
[20] Lu XZ, Tian Y, Sun CJ, Zhang SH. Development and application of a high-performance triangular shell element and an explicit algorithm in OpenSees for strongly nonlinear analysis. CMES-Comput Model Eng Sci 2019;120(3):561–82.
[21] Pham AT, Tan KH, Yu J. Numerical investigations on static and dynamic responses of reinforced concrete sub-assemblages under progressive collapse. Eng Struct 2017;149:2–20.
[22] Lisha Wang, Song Cen, Linlin Xie, Xinzheng Lu. Shear wall model based on a novel large deformation plate shell element and its application in OpenSees[J]. Eng Mech 2016;33(03):47–54.
[23] Kolozvari K, Orakcal K, Wallace JW. Modeling of cyclic shear-flexure interaction in reinforced concrete structural walls. I: Theory. J Struct Eng, ASCE 2015;141(5): 04014135.
[24] Noh G, Bathe K. An explicit time integration scheme for the analysis of wave propagations. Comput Struct 2013;129:178–93.
[25] Jiang J, Usmani A. Modeling of steel frame structures in fire using Opensees. Comput Struct 2013;118:90–9.
[26] Lu XZ, Xie LL, Guan H, Huang YL, Lu X. A shear wall element for nonlinear seismic analysis of super-tall buildings using Opensees. Finite Elem Anal Des 2015;98: 14–25.